# Coherence Decay in Turbulent Jets by Stochastic Modelling Under Location Uncertanty

Gilles Tissot, André Cavalieri, Tim Colonius, Peter Jordan, Etienne Mémin

▶ **To cite this version:**

Gilles Tissot, André Cavalieri, Tim Colonius, Peter Jordan, Etienne Mémin. Coherence Decay in Turbulent Jets by Stochastic Modelling Under Location Uncertanty. 2024 - 30th AIAA/CEAS Aeroacoustics Conference, Jun 2024, Rome, Italy. pp.1-17, 10.2514/6.2024-3204 . hal-04632589

**HAL Id: hal-04632589**

**https://inria.hal.science/hal-04632589v1**

Submitted on 2 Jul 2024

**HAL** is a multi-disciplinary open access archive for the deposit and dissemination of scientific research documents, whether they are published or not. The documents may come from teaching and research institutions in France or abroad, or from public or private research centers.

L'archive ouverte pluridisciplinaire **HAL**, est destinée au dépôt et à la diffusion de documents scientifiques de niveau recherche, publiés ou non, émanant des établissements d'enseignement et de recherche français ou étrangers, des laboratoires publics ou privés.

Distributed under a Creative Commons Attribution 4.0 International License

# Coherence decay in turbulent jets by stochastic modelling under location uncertainty

G. Tissot* and E. Mémin
*Centre INRIA de l'Université de Rennes, IRMAR – UMR CNRS 6625, 35042 Rennes, France.*

André V. G. Cavalieri
*Department of Aerospace Engineering, Instituto Tecnológico de Aeronáutica, 12228-900 São José dos Campos, Brazil.*

Tim Colonius
*Department of Mechanical and Civil Engineering, California Institute of Technology, Pasadena, CA 91125, USA.*

Peter Jordan
*Institut Pprime, CNRS / Université de Poitiers /ENSMA, 86962 Futuroscope Chasseneuil, France.*

**Coherence decay has been understood to be a key quantity to predict acoustic noise emitted by wavepackets in subsonic turbulent jets. Frequency-domain frameworks such as *input-output* and *resolvent* analyses are able to predict accurately the spatial structure of wavepackets turbulent flows compared to coherent structures educed from simulation data (as for example identified using spectral proper orthogonal, SPOD). However, at least at reduced-order, they are unable to capture two-point statistics such as coherence. A missing piece is the modelling of variability induced by the turbulence, which jitters (disorganises) the coherent structures and leads to stronger noise radiation. The aim of the present study is to consider the impact of turbulence on jet wavepackets through stochastic modelling under location uncertainty. This framework considers the conservation of mass and momentum of fluid parcels submitted to a stochastic transport, representing here the effect of turbulence. By linearising the resulting generalised stochastic Navier–Stokes equations and expressing it in the Fourier domain, a stochastic linear model (SLM) is obtained. We explore in this paper that ability of SLM to predict the two point coherence of the wavepackets in turbulent jets, and show its impact on acoustic emissions.**

## I. Introduction

In turbulent jets, wavepackets are a major source of acoustic noise emissions, at least at low angle sound radiation from the jet axis [1, 2]. Their amplitude can be predicted by linear models, such as PSE [3], and more accurately by input-output frameworks, such as resolvent analysis [4, 5]. In supersonic jets, these wavepackets radiate in Mach waves, then right acoustic emission can be obtained from simplified models [6]. However, in subsonic jets, these waves are subject to destructive interferences of the regular wave-trains solution of the linear models. In a turbulent jet, these wavepackets jitter. They are disorganised [7] by their interactions with the turbulent field, and the acoustic emission is strongly intensified by the breaking of destructive interferences. It has been shown [8, 9] that two points statistics, such as the coherence have to be informed in the models of acoustic propagation in order to obtain the right acoustic levels.

The missing piece is identified: coherence decay measures the irregularity of the wavepackets and drives the interference mechanisms. This loss of coherence is caused by the interactions of these wavepackets with the turbulent field. These interactions are non-linear and intrinsically couple frequencies and wavenumbers. In the context of reduced order modelling, it is out of question to conduct high fidelity numerical simulations and simplified models accounting for these interactions are required. As a consequence, obtaining the two-point coherence is a challenging task.

Coherence is a statistical quantity. The approach, that we consider in the present study, is to model the turbulent field by a stochastic variable, informed by its statistics. We consider the impact of turbulence on the wavepacket (solution of the model), through a stochastic transport. We rely for this on a framework, the stochastic modelling under location uncertainty (SLU), introduced by Mémin [10]. The principle is to write the conservation of mass and momentum on fluid parcels submitted to a stochastic transport by the resolved velocity, perturbed by an unresolved (turbulent)

*Gilles.Tissot@inria.fr

velocity component, which is modelled by the derivative of a Brownian motion. Following Ito stochastic calculus, a generalisation of the Navier–Stokes equations is obtained. This framework has widely and successfully been employed for turbulence modelling [11, 12], data assimilation [13–15] and geophysical flows modelling [16–21]. This SLU system accounts for the transport by the stochastic noise, the stochastic diffusion and a drift velocity induced by the inhomogeneity of the stochastic noise. In the context of coherent structures in channel flows, Tissot et al. [22, 23] have expressed the SLU system in the Fourier domain. In this context, the stochastic noise represents the unresolved turbulent field perturbing the coherent structures through a stochastic transport. This framework, named stochastic linear model (SLM) – and forced stochastic linear model (FSLM) when non-linear forcing term has been introduced – has demonstrated better predictions of coherent structures in the buffer and logarithmic layer than input-output resolvent analysis, with and without eddy viscosity. Some similar attempts have been performed in the context of turbulent channel flows by combining eddy viscosity with forcing models [24], but without the SLU framework a strong connection between these two modelling features is missing.

We propose in the present paper to adapt the SLM in order to predict coherence decay of wavepackets in a $M = 0.4$ turbulent jet at $Re = 450000$. The modelling is driven by the intuition that the jitter of wavepackets, caused by turbulent non-linear interactions, can be fairly represented by a stochastic transport through the stochastic under location uncertainty framework. We aim at deriving a model as uninformed by the data as possible. For this, we rely on a Reynolds averaged Navier–Stokes (RANS) model, which provides the mean flow over which the linearisation is performed and eddy viscosity used for defining the stochastic diffusion. The stochastic noise defined in the Fourier space is build based on suboptimal resolvent modes, following the idea that such a basis span turbulent perturbations which are likely present in the flow. To target coherence decay, the incompressible assumption is performed in the present paper. The results are compared with large eddy simulation (LES) data. We finally propagate the acoustic field through a Kirchhoff surface based formulations [as in 9, 25]. Despite some rough approximations, it highligts the importance of two-point statistics for acoustic emissions, and opens new perspectives for stochastic modelling of subsonic turbulent jet noise.

In section II notations and the flow configuration are presented. A brief recall of the resolvent analysis is given in section III. It will constitute de standard models to which the stochastic model presented in section IV will be compared. Numerical results are shown in section V, where a focus is first made on the turbulent field, then on its impact on the acoustic emissions. Concluding remarks and perspectives are given in VI.

## II. Notations and flow configuration

In this paper, we consider a jet flow, at $M = U_j/a_j = 0.4$ and $Re = \rho_j U_j D/\mu_j = 450000$, where $M$ is the Mach number, $U_j$, $a_j$ $\rho_j$ and $\mu_j$ are respectively the velocity, sound speed, density and dynamic viscosity at the jet centerline at the nozzle exit. $Re$ is the Reynolds number and $D$ the jet diameter. The Strouhal number $St = fD/U_j$ is the frequency $f$ adimensionalised by the jet velocity and diameter. The cylindrical coordinates are noted $\boldsymbol{x} = (x, r, \theta)^T$ associated respectively with the axial, radial and azimuthal directions. The size of the cylindrical physical domain $\Omega$ is $[0 : L_x] \times [0 : Lr] \times [0 : 2\pi]$, with $L_x = 25$ and $L_r = 5$. The flow field solution is $\boldsymbol{q} = (u, v, w, p)^T$ representing the axial, radial and azimuthal velocity components and the pressure, respectively. The velocity field is decomposed in a time-averaged flow and a fluctuation $\boldsymbol{u} = \overline{\boldsymbol{u}} + \boldsymbol{u'}$ with $\overline{\boldsymbol{u}} = (\overline{U}, \overline{V}, 0)^T$. Fourier decomposition of the fluctuation are considered in time $t$ and in the azimuthal directions, with $\hat{\boldsymbol{q}}_{m,\omega}(\boldsymbol{x}) = \frac{1}{2\pi}\int_0^{2\pi}\int_0^{\infty} \boldsymbol{q'}(\boldsymbol{x}, t)e^{-i(2\pi m\theta-\omega t)}\,\mathrm{d}\omega\,\mathrm{d}\theta$ and $\boldsymbol{q'}(\boldsymbol{x}, t) = \frac{1}{2\pi}\sum_m \int_{-\infty}^{\infty} \hat{\boldsymbol{q}}_{m,\omega}(\boldsymbol{x})e^{i(2\pi m\theta-\omega t)}\mathrm{d}\omega$, where $\omega$ is the angular frequency and $m$ the azimuthal wavenumber. In the Fourier domain, the 2D coordinates are still noted $\boldsymbol{x} = (x, r)^T$ by abuse.

## III. Resolvent analysis

Resolvent analysis [26, 27] is today widely employed for the linear analysis of turbulent flows. It connects, in the frequency domain, an orthonormal basis of the most amplified flow responses to the associated most responsive forcings, constituting an optimal basis onto which the non-linearities can be projected to obtain a reduced-order representation of the actual flow response. Since this non-linear term is issued from a convolution over all frequencies and wave numbers, it is unknown; and treated as a forcing term, referred to as *non-linear forcing*. Cross spectral density (CSD) tensor of the solution – allowing to obtain the coherence –, can be connected to the CSD of the non-linear forcing through the resolvent operator [28]. Without information from data, the most parsimonious assumption is to consider that the non-linear forcing is a Gaussian white noise, which is unlikely an accurate representation, but is some cases [29] lead to fair modelling of the main traits of the response. The CSD of the response can then be easily predicted at first

approximation. This constitutes in the present paper a methodology that we aim at enriching with the SLU framework. In this section, we then briefly recall the resolvent analysis, and the methodology to build a reduced-order representation of the resolvent-based CSD.

We consider the deterministic incompressible Navier–Stokes equations, linearised over the mean flow $\overline{\boldsymbol{q}} = (\overline{U}, \overline{V}, 0, \overline{P})^T$, and written formally

$$(\boldsymbol{A}_{m,\omega} - i\omega\boldsymbol{E})\hat{\boldsymbol{q}}_{m,\omega} = \boldsymbol{L}_{m,\omega}\hat{\boldsymbol{q}}_{m,\omega} = \boldsymbol{N}_{m,\omega}(\boldsymbol{u'}), \tag{1}$$

where $\boldsymbol{A}_{m,\omega}$ is the Fourier transform of the linearised Navier–Stokes operator, and $\boldsymbol{E}$ is a diagonal matrix with 1 and 0 values for velocity and pressure components respectively. $\boldsymbol{L}_{m,\omega}^{-1} = (\boldsymbol{A}_{m,\omega} - i\omega\boldsymbol{E})^{-1}$ is the resolvent of the operator $\boldsymbol{A}_{m,\omega}$. Formally, the non-linear term $\boldsymbol{N}_{m,\omega}(\boldsymbol{u'})$ can be considered as a right-hand side of equations (1). However, the Fourier transform of a product is a convolution, which results in an integral over all frequency-wavenumbers, which is incompatible with a prediction for an "isolated" frequency-wavenumber combination. The goal of resolvent analysis is to explore the response of the linear operator $\boldsymbol{L}_{m,\omega}$ to non-linearities treated as an external forcing. In what follows we will consider the discretised form of equation (1), which, by replacing $\boldsymbol{N}_{m,\omega}$ by an external forcing, becomes

$$\boldsymbol{L}_{m,\omega}\hat{\boldsymbol{q}}_{m,\omega} = \boldsymbol{B}\hat{\boldsymbol{f}}_{m,\omega}. \tag{2}$$

Since non-linear terms act only on the momentum equations, and since in incompressible flows the state of the system can be characterised only knowing the velocity, we define input and output matrices respectively as

$$\boldsymbol{B} = \begin{pmatrix} \mathbb{I} & 0 & 0 \\ 0 & \mathbb{I} & 0 \\ 0 & 0 & \mathbb{I} \\ 0 & 0 & 0 \end{pmatrix} \quad \text{and} \quad \boldsymbol{H} = \begin{pmatrix} \mathbb{I} & 0 & 0 & 0 \\ 0 & \mathbb{I} & 0 & 0 \\ 0 & 0 & \mathbb{I} & 0 \end{pmatrix}. \tag{3}$$

The output matrix $\boldsymbol{H}$ thus extracts only the velocity components, which may be combined with the standard $L^2(\Omega, \mathbb{R}^3)$ inner product to induce a norm corresponding to the kinetic energy. The response to a harmonic forcing $\hat{\boldsymbol{f}}_{m,\omega}$ is $\boldsymbol{H}\hat{\boldsymbol{q}}_{m,\omega} = \boldsymbol{H}\boldsymbol{L}_{m,\omega}^{-1}\boldsymbol{B}\hat{\boldsymbol{f}}_{m,\omega}$. The frequency response operator is thus defined from the resolvent operator, $\boldsymbol{L}_{m,\omega}^{-1}$, as $\boldsymbol{R}_{m,\omega} = \boldsymbol{H}\boldsymbol{L}_{m,\omega}^{-1}\boldsymbol{B}$. We then search for the forcing that maximises

$$\max_{\hat{\boldsymbol{f}}_{m,\omega}} \frac{\|\boldsymbol{H}\hat{\boldsymbol{q}}_{m,\omega}\|_W^2}{\|\hat{\boldsymbol{f}}_{m,\omega}\|_W^2} = \frac{\|\boldsymbol{R}_{m,\omega}\hat{\boldsymbol{f}}_{m,\omega}\|_W^2}{\|\hat{\boldsymbol{f}}_{m,\omega}\|_W^2}. \tag{4}$$

The maximisation of the Rayleigh quotient (4) can be achieved by means of the following singular value decomposition,

$$\boldsymbol{W}^{1/2}\boldsymbol{R}_{m,\omega}\boldsymbol{W}^{-1/2} = \boldsymbol{U}_r\boldsymbol{\Sigma}_r\boldsymbol{V}_r^*, \tag{5}$$

where $\boldsymbol{W}^{1/2}$ is defined by the Cholesky decomposition $\boldsymbol{W} = \boldsymbol{W}^{1/2}(\boldsymbol{W}^{1/2})^*$, with $\boldsymbol{W}$ the diagonal matrix containing the quadrature weighs approximating the space integral over $\Omega$, $\boldsymbol{U}_r = (\boldsymbol{U}_{r,1}, \ldots, \boldsymbol{U}_{r,N})$ and $\boldsymbol{V}_r = (\boldsymbol{V}_{r,1}, \ldots, \boldsymbol{V}_{r,N})$ are orthonormal matrices and $\boldsymbol{\Sigma}_r = \mathrm{diag}(s_1, \ldots, s_N)$ is a diagonal matrix. We define the optimal forcing modes as, $\boldsymbol{\Psi}_i^{\text{resolvent}} = \boldsymbol{W}^{-1/2}\boldsymbol{V}_{r,i}$, and the associated optimal response modes (also referred to as resolvent modes in the following) as, $\boldsymbol{\Phi}_i^{\text{resolvent}} = \boldsymbol{W}^{-1/2}\boldsymbol{U}_{r,i}$. We write the matrices $\boldsymbol{\Psi}^{\text{resolvent}}$ and $\boldsymbol{\Phi}^{\text{resolvent}}$ the matrices gathering in columns the $N_{\text{modes}}$ first resolvent forcing and response modes, respectively. The singular values, $s_i$, diagonal elements of $\boldsymbol{\Sigma}_r$ sorted in descending order, indicate the $N_{\text{modes}}$ first gains associated with forcing-response mode pairs. Indices $(m, \omega)$ are dropped here to lighten the notations.

As shown in Towne et al. [28], the CSD, defined as

$$\boldsymbol{S}_{m,\omega}^{\boldsymbol{uu}}(\boldsymbol{x}, \boldsymbol{x'}) = \mathbb{E}(\hat{\boldsymbol{u}}_{m,\omega}(\boldsymbol{x})\hat{\boldsymbol{u}}_{m,\omega}^*(\boldsymbol{x'})), \tag{6}$$

with $\cdot^*$ denoting the transpose-conjugate operation, can be reexpressed using the resolvent operator

$$\begin{aligned} \boldsymbol{S}_{m,\omega}^{\boldsymbol{uu}}(\boldsymbol{x}, \boldsymbol{x'}) &= \mathbb{E}\left(\left(\boldsymbol{R}_{m,\omega}\hat{\boldsymbol{f}}_{m,\omega}\right)(\boldsymbol{x})\left(\hat{\boldsymbol{f}}_{m,\omega}^*\boldsymbol{R}_{m,\omega}^*\right)(\boldsymbol{x'})\right) \\ &= \left(\boldsymbol{R}_{m,\omega}\mathbb{E}\left(\hat{\boldsymbol{f}}_{m,\omega}\hat{\boldsymbol{f}}_{m,\omega}^*\right)\boldsymbol{R}_{m,\omega}^*\right)(\boldsymbol{x}, \boldsymbol{x'}) \\ &= \boldsymbol{R}_{m,\omega}\boldsymbol{S}_{m,\omega}^{\boldsymbol{ff}}\boldsymbol{R}_{m,\omega}^*, \end{aligned} \tag{7}$$

where $\boldsymbol{S}^{ff}_{m,\omega} = \mathbb{E}(\hat{\boldsymbol{f}}_{m,\omega}\hat{\boldsymbol{f}}^{*}_{m,\omega})$ stands for the CSD of the non-linear forcing. The resolvent operator thus connects the CSD of the forcing with the CSD of the response.

Assuming that the CSD of the non-linear forcing is identity, *i.e.* the non-linear terms acts as a Gaussian white noise, a reduced-order representation of the CSD can be computed using the resolvent modes

$$\boldsymbol{S}^{\boldsymbol{uu},\text{resolvent}}_{m,\omega}(\boldsymbol{x},\boldsymbol{x}') = \sum_{k=1}^{N_{\text{modes}}} s_i^2 \boldsymbol{\Phi}^{\text{resolvent}}_{k}(\boldsymbol{x}) \left(\boldsymbol{\Phi}^{\text{resolvent}}_{k}\right)^{*}(\boldsymbol{x}'). \tag{8}$$

Coherence $\gamma^2$ between two points $(\boldsymbol{x},\boldsymbol{x}')$ and two components $(i,j)$, can be then estimated from the CSD

$$(\gamma^{ij}_{m,\omega})^2(\boldsymbol{x},\boldsymbol{x}') = \frac{|\boldsymbol{S}^{ij}_{m,\omega}(\boldsymbol{x},\boldsymbol{x}')|^2}{\boldsymbol{S}^{ii}_{m,\omega}(\boldsymbol{x},\boldsymbol{x})\boldsymbol{S}^{jj}_{m,\omega}(\boldsymbol{x}',\boldsymbol{x}')}. \tag{9}$$

A way to take into account a part of the non-linearities is to consider a triple decomposition of the velocity field [30], where the Reynolds stresses induced by the incoherent part of the turbulent velocity is modelled by an eddy-viscosity. The modification of the linearised operator by replacing molecular diffusion with eddy diffusion is noted $\boldsymbol{L}^{\nu_T}_{m,\omega}$. Resolvent analysis and coherence predictions can thus be conducted, and referred to as *eddy resolvent*, and noted in the following $\bullet^{\nu_T\text{-resolvent}}$. Such a modelling has been employed in the context of resolvent analysis to improve the ability of resolvent analysis to reproduce the coherent structures in the flow [31, 32]; this is at the price of a modelling effort on the used eddy viscosity.

In the following, the resolvent analysis referred to as *without eddy viscosity* has in fact been performed at $Re = 30000$ for convergence purposes, which may be considered as a small constant background eddy viscosity.

## IV. Stochastic modelling under location uncertainty

Loss of coherence of wavepackets is intrinsically caused by their interactions with the turbulence, which has a statistical effect on averaged quantities, alike eddy diffusion, but as well a variability between realisations. These interactions are non-linear and are induced by advection phenomena, which have likely a structure deviating from and additive Gaussian white noise. In the present paper, we aim at introducing the stochastic modelling at a more fundamental level than an additive stochastic non-linear forcing, and considering the stochastic transport of conserved quantities by a resolved velocity field perturbed by a random turbulent fluctuation. We first present the SLU framework, and then the linearised model used for obtaining a CSD from the stochastic model.

### A. Navier–Stokes equations under location uncertainty

The principle is to formulate conservation laws for transport by a resolved time-differentiable velocity perturbed by the derivative of a Brownian motion. Under these hypotheses, the conservation of mass and momentum lead to a stochastic version of the Navier–Stokes equations written for an infinitesimal time increment.

The displacement $\boldsymbol{X}(\boldsymbol{x},t)$ of a particle is written in a differential form

$$\mathrm{d}\boldsymbol{X}(\boldsymbol{x},t) = \boldsymbol{u}(\boldsymbol{x},t)\mathrm{d}t + (\boldsymbol{\sigma}_t \mathrm{d}\boldsymbol{B}_t)(\boldsymbol{x}), \tag{10}$$

where $\boldsymbol{u}$ is a time-differentiable velocity component, and $\mathrm{d}\boldsymbol{B}_t$ is the increment of a Brownian motion. The correlation operator $\boldsymbol{\sigma}_t$ is an integral operator such that

$$(\boldsymbol{\sigma}\mathrm{d}\boldsymbol{B}_t)^i(\boldsymbol{x}) = \int_\Omega \check{\boldsymbol{\sigma}}^{ij}(\boldsymbol{x},\boldsymbol{x}',t)\mathrm{d}\boldsymbol{B}^j_t(\boldsymbol{x}')\,\mathrm{d}\boldsymbol{x}', \tag{11}$$

where $\check{\boldsymbol{\sigma}}$ is a kernel specifying the space correlations (eventually smoothly time-dependent) of the unresolved displacement field. The transport noise $\boldsymbol{\sigma}_t\mathrm{d}\boldsymbol{B}_t$ is then assumed correlated in space and decorrelated in time. Unlike other velocity field decompositions, which are based on the definition of an averaged operator (such as ensemble or phase average) separating the averaged field and its fluctuation, here the separation is based on the time regularity – at the time scale of the physical processes at play. The displacement is separated into a time-differentiable and a martingale part. It can be noticed that turbulent signals, due to their multi-scale nature, can fairly be represented as such, once a time scale of the increment is specified.

Associated with $\boldsymbol{\sigma}_t$, we define the variance tensor $\boldsymbol{a}$ such that

$$\boldsymbol{a}_{ij}(\boldsymbol{x})\mathrm{d}t = \mathbb{E}\left( (\boldsymbol{\sigma}_t \mathrm{d}\boldsymbol{B}_t)^i (\boldsymbol{x}) \ (\boldsymbol{\sigma}_t \mathrm{d}\boldsymbol{B}_t)^j (\boldsymbol{x}) \right). \tag{12}$$

Using the Ito-Wentzell formula, conservation of mass and momentum subject to a stochastic transport leads to a stochastic version of the incompressible Navier–Stokes equations [10, 16], referred to as *under location uncertainty*:

$$\begin{aligned} &\mathrm{d}_t \boldsymbol{u} + (\boldsymbol{u}_d \cdot \nabla)\,\boldsymbol{u}\,\mathrm{d}t + (\boldsymbol{\sigma}_t \mathrm{d}\boldsymbol{B}_t \cdot \nabla)\,\boldsymbol{u} = -\nabla\,(p_t\,\mathrm{d}t + \mathrm{d}p_t) + \frac{1}{Re}\nabla\cdot(\nabla \boldsymbol{u})\ \mathrm{d}t + \nabla\cdot\left(\frac{1}{2}\boldsymbol{a}\nabla\boldsymbol{u}\right)\mathrm{d}t + \frac{1}{Re}\nabla\cdot(\nabla\boldsymbol{\sigma}_t\mathrm{d}\boldsymbol{B}_t) \\ &\nabla\cdot\boldsymbol{u}_d = 0; \quad \nabla\cdot\boldsymbol{\sigma}_t = 0, \\ &\boldsymbol{u}_d = \boldsymbol{u} - \frac{1}{2}\nabla\cdot\boldsymbol{a}. \end{aligned} \tag{13}$$

Compared to the deterministic case, additional terms naturally appear from Ito stochastic calculus: a stochastic diffusion (alike an eddy viscosity), an effective drift velocity accounting for turbophoresis and the transport by the noise. A stochastic contribution to the pressure and viscous stresses emerge as well. The velocity $\boldsymbol{u}_d$ is called *drift velocity*, and it can be remarked that mass conservation and incompressibility enforce this drift velocity and the noise to be solenoidal. This framework has the advantage to be energetically consistent since the stochastic diffusion compensates exactly the energy brought by the noise [16]. Moreover, these additional terms emerge directly from stochastic calculus, and are not issued from additional closure modelling, such as the Boussinesq assumption.

### B. Stochastic linear model

In Tissot et al. [22, 23], stochastic modelling under location uncertainty (SLU) has been employed to model coherent structures in turbulent channel flows. In the present work, we aim at modelling the impact of turbulence on wavepackets using SLU in order to predict their coherence decay. The analysis is similar to Tissot et al. [23] but cast in cylindrical configuration. For stationary jets from round nozzles, the SLU model is expressed in the Fourier domain in time and azimuthal directions. The stochastic linear model (SLM) system is written as follows:

$$\begin{aligned} &\begin{pmatrix} A_{\text{adv}}(\cdot) + \frac{\partial U}{\partial x} - D_{xx}(\cdot) & \frac{\partial U}{\partial r} - D_{xr}(\cdot) & 0 & \frac{\partial \cdot}{\partial x} \\ \frac{\partial V}{\partial x} - D_{rx}(\cdot) & A_{\text{adv}}(\cdot) + \frac{\partial V}{\partial r} - D_{rr}(\cdot) & 0 & \frac{\partial \cdot}{\partial r} \\ 0 & 0 & A_{\text{adv}}(\cdot) + \frac{1}{r}V - D_{zz}(\cdot) & im\frac{1}{r} \\ \frac{\partial \cdot}{\partial x} & \frac{1}{r}\frac{\partial r\cdot}{\partial r} & im\frac{1}{r} & 0 \end{pmatrix} \begin{pmatrix} \hat{u}_{m,\omega} \\ \hat{v}_{m,\omega} \\ \hat{w}_{m,\omega} \\ \hat{p}_{m,\omega} \end{pmatrix} \\ &= \begin{pmatrix} -(\dot{\boldsymbol{\xi}}_{m,\omega})_x \frac{\partial U}{\partial x} - (\dot{\boldsymbol{\xi}}_{m,\omega})_r \frac{\partial U}{\partial r} + \frac{1}{Re}\nabla\cdot(\nabla(\dot{\boldsymbol{\xi}}_{m,\omega})_x) \\ -(\dot{\boldsymbol{\xi}}_{m,\omega})_x \frac{\partial V}{\partial x} - (\dot{\boldsymbol{\xi}}_{m,\omega})_r \frac{\partial V}{\partial r} + \frac{1}{Re}\nabla\cdot(\nabla(\dot{\boldsymbol{\xi}}_{m,\omega})_y) \\ \frac{1}{Re}\nabla\cdot(\nabla(\dot{\boldsymbol{\xi}}_{m,\omega})_z) \\ 0 \end{pmatrix}, \end{aligned} \tag{14}$$

with $A_{\text{adv}}(\cdot) = -i\omega + U_d\frac{\partial \cdot}{\partial x} + V_d\frac{\partial \cdot}{\partial r}$, and $D(\cdot) = \frac{1}{Re}\nabla\cdot(\nabla(\cdot)) + \frac{1}{2}\nabla\cdot(\boldsymbol{a}\nabla(\cdot))$. The element $D_{ij}(\cdot)$ is the component $i$ of the diffusive term associated with the $j$-th velocity field component. Here, divergence and gradient in cylindrical coordinates are written formally $\nabla\cdot$ and $\nabla$, respectively. The drift mean flow is $(U_d, V_d, 0)^T = (\overline{U}, \overline{V}, 0)^T - \frac{1}{2}\nabla\cdot\boldsymbol{a}$. The Fourier transform of $\boldsymbol{\sigma}_t\mathrm{d}\boldsymbol{B}_t$ is noted $\mathrm{d}\boldsymbol{\xi}_{m,\omega}$, and the associated velocity Fourier component $\dot{\boldsymbol{\xi}}_{m,\omega} = \mathrm{d}\boldsymbol{\xi}_{m,\omega}/\mathrm{d}t$ is a standard centered Gaussian white noise convolved with the space-Fourier transform of $\boldsymbol{\sigma}_t$. It has to be stressed that $\hat{\boldsymbol{q}}_{m,\omega}$ is a stochastic variable, rendering straightforward the definition of the CSD, $\boldsymbol{S}^{\text{SLM}}_{m,\omega}$, through the expectation operator:

$$\boldsymbol{S}^{\text{SLM}}_{m,\omega}(\boldsymbol{x},\boldsymbol{x}') = \mathbb{E}\left(\hat{\boldsymbol{q}}_{m,\omega}(\boldsymbol{x})\hat{\boldsymbol{q}}^*_{m,\omega}(\boldsymbol{x}')\right). \tag{15}$$

The SLU model allows us to obtain a CSD tensor associated with linear evolution of wavepackets submitted to a stochastic transport – representing the effect of turbulence on the solution.

In practice, eigenfunctions $\boldsymbol{\Phi}^{\text{SLM}}_{k,m,\omega}(\boldsymbol{x})$ and eigenvalues $\lambda^{\text{SLM}}_{k,m,\omega}$ of the CSD are computed through a SVD procedure, as in Tissot et al. [23]. First, the noise is decomposed onto a basis $\dot{\boldsymbol{\xi}}_{m,\omega} = \sum_{k=1}^{N_\sigma} c_k \boldsymbol{\Phi}^\sigma_k \eta_k$, where $(c_k, \boldsymbol{\Phi}^\sigma_k)$ are amplitude

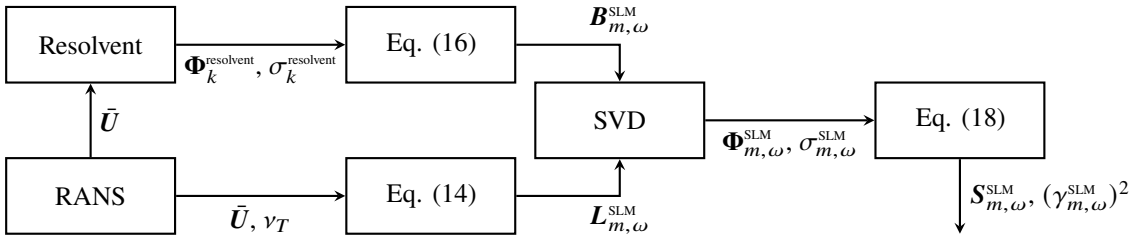


**Fig. 1 Schematic representation of the SLM procedure.**

coefficients and normalised vectors defined in section IV.C, and $\eta_k$ are standard centered Gaussian white noises. We define the matrix $\widetilde{\boldsymbol{\Phi}} = (c_1\boldsymbol{\Phi}_1^{\sigma}, \cdots, c_{N_\sigma}\boldsymbol{\Phi}_{N_\sigma}^{\sigma})$. Then, a SLM input matrix can be defined as

$$\boldsymbol{B}^{\text{SLM}} = \begin{pmatrix} -(\widetilde{\boldsymbol{\Phi}})_x \dfrac{\partial U}{\partial x} - (\widetilde{\boldsymbol{\Phi}})_r \dfrac{\partial U}{\partial r} + \frac{1}{Re}\nabla\cdot(\nabla(\widetilde{\boldsymbol{\Phi}})_x) \\ -(\widetilde{\boldsymbol{\Phi}})_x \dfrac{\partial V}{\partial x} - (\widetilde{\boldsymbol{\Phi}})_r \dfrac{\partial V}{\partial r} + \frac{1}{Re}\nabla\cdot(\nabla(\widetilde{\boldsymbol{\Phi}})_r) \\ \frac{1}{Re}\nabla\cdot(\nabla(\widetilde{\boldsymbol{\Phi}})_\theta) \\ 0 \end{pmatrix}, \tag{16}$$

acting on the input vector $\boldsymbol{\eta} = (\eta_1, \ldots, \eta_{N_\sigma})^T$. The linear stochastic system (14) can be written compactly:

$$\boldsymbol{L}_{m,\omega}^{\text{SLM}}\hat{\boldsymbol{q}}_{m,\omega} = \boldsymbol{B}^{\text{SLM}}\boldsymbol{\eta}. \tag{17}$$

The SLM eigenfunctions $\boldsymbol{\Phi}_{k,m,\omega}^{\text{SLM}}(\boldsymbol{x})$ and eigenvalues $\lambda_{k,m,\omega}^{\text{SLM}}$ are obtained as in resolvent analysis described in section III, but with the system (17) and taking the output matrix unchanged $\boldsymbol{H}^{\text{SLM}} = \boldsymbol{H}$. The CSD is then approximated by a $N_{\text{modes}}$ modes truncation of its spectral representation

$$\boldsymbol{S}_{m,\omega}^{\text{SLM}}(\boldsymbol{x},\boldsymbol{x}') \approx \sum_{k=0}^{N_{\text{modes}}} \lambda_{k,m,\omega}^{\text{SLM}}(\boldsymbol{\Phi}_{k,m,\omega}^{\text{SLM}})(\boldsymbol{x})(\boldsymbol{\Phi}_{k,m,\omega}^{\text{SLM}})^*(\boldsymbol{x}'), \tag{18}$$

and thus the coherence $(\gamma^{\text{SLM}})^2$ as in (9).

### C. Definition of the noise

In the SLU formalism, $\boldsymbol{\sigma}_t \mathrm{d}\boldsymbol{B}_t$ is unresolved and specified in the modelling process. In the present paper, up to some modelling choices, we aim at obtaining a model as exempt from information coming from data as possible. To that end, we rely on the solution of a RANS computation, and the output of a resolvent analysis (without eddy viscosity) to define the noise. A schematic representation of the procedure is shown in figure 1, and the procedure is explained in detail in the present section.

A steady RANS $k-\epsilon$ calculation allows us to obtain a mean flow velocity field. Numerical details and consistency of this mean flow with the LES database is described in Pickering et al. [32]. This mean flow constitutes the linearisation point of the problem.

To define the noise variance and $\boldsymbol{\sigma}_t \mathrm{d}\boldsymbol{B}_t$, it has to be remarked that the variance tensor $\boldsymbol{a}$ is the variance of $\boldsymbol{\sigma}_t \mathrm{d}\boldsymbol{B}_t$ defined in the temporal domain. However in (14), the Fourier transform $\mathrm{d}\boldsymbol{\xi}_{m,\omega}$ of $\boldsymbol{\sigma}_t \mathrm{d}\boldsymbol{B}_t$ is involved in the right-hand-side (RHS). Despite the strong connection between $\boldsymbol{a}$ and $\boldsymbol{\sigma}_t \mathrm{d}\boldsymbol{B}_t$ in (12), which provides the property that the energy brought by the noise is exactly compensated by the stochastic diffusion; this constraint is lost numerically due to the formulation in the Fourier domain. This is the price to pay to perform frequency-by-frequency calculations. This balance remains only at the theoretical level, but is not accessible in practice while all frequency-wavenumbers are not computed. As a consequence, we model $\mathrm{d}\boldsymbol{\xi}_{m,\omega}$ and $\boldsymbol{a}$ separately, similarly as in Tissot et al. [23].

First, since the stochastic diffusion tensor $\boldsymbol{a}$ plays the role of an eddy viscosity, we model it using the eddy viscosity $\nu_T$ from the RANS model $\boldsymbol{a} = c\nu_T\mathbb{I}$, with the scaling constant $c = 0.2$ determined in [32, section 7.1] such that $\nu_T$-resolvent modes correspond at best with SPOD modes. This choice is two fold. First, it allows to keep consistency with the LES database, accounting for the fact that the eddy-viscosity term determined to match the mean-flow has not necessarily the same value than the one acting at the frequency considered to model the generalised Reynolds stress

[24, 33]. Secondly, it allows to perform fair comparisons with standard $\nu_T$-resolvent by comparing models having exactly the same eddy diffusion. We can note that in the whole procedure, the use of the constant $c$ is the only place where LES data are informing the stochastic model, through the best correspondence between $\nu_T$-resolvent and SPOD modes.

The stochastic noise $\mathrm{d}\boldsymbol{\xi}_{m,\omega}$ represents, at the azimuthal wavenumber/frequency $(m, \omega)$, incoherent turbulent flow structures. It is represented on a projection basis $\boldsymbol{\Phi}^{\sigma}$. At this frequency, the flow structures which are likely present should project strongly on optimal resolvent response modes. As in Tissot et al. [23], we represent $\mathrm{d}\boldsymbol{\xi}_{m,\omega}$ on the resolvent basis (without eddy viscosity), discarding the first coherent wavepacket mode (which is the dominant coherent structure and not really an incoherent turbulent variability mode). In such a way, the noise basis is composed by Orr suboptimal modes [4] representative of incoherent small scale turbulence. We thus define $\boldsymbol{\Phi}^{\sigma}_{k} = \boldsymbol{\Phi}^{\text{resolvent}}_{k+1}$ and $c_k = s^{\text{resolvent}}_{k+1}$.

The modelling hypothesis underlying these choices are that, the resolvent suboptimal modes, integrated over all frequencies/wavenumbers are representative of the turbulent fluctuations making the wavepacket jitter and inducing the eddy diffusion predicted by the RANS model. There are two distinct ideas behind this statement. The first point comes from the observation that, the resolvent modes in jets show a dominance of the first mode of Kelvin-Helmholtz-type [4] suggesting a separation between incoherent turbulent field inducing eddy diffusion and a dominant wavepacket. The second idea is sustained by the fact that wavepackets are sensitive to Orr-like perturbations [34], such that a noise defined as presented here may likely be able to induce an efficient coherence decay.

## V. Results

In this section, the power spectral densities (PSD) and cross spectral densities (CSD) obtained respectively by resolvent analysis (with and without eddy viscosity) and by SLM are compared with LES data. The large eddy simulation database is the ($M = 0.4$, $Re = 450000$) jet computed using the flow solver "Charles", in Brès et al. [35]. Numerical details of the SPOD are given in Schmidt et al. [4]. Resolvent and SLM are discretised using 4-th order finite differences on a stretched Arakawa-B grid of size ($N_x = 1024$, $N_r = 200$). Order 4 interpolations are performed between the $p$-grid and $(u, v)$-grid. A 20-point stencil optimized filter is added to $\boldsymbol{B}$ for the resolvent analysis, in such a way to forbid spurious aliased forcings to the Kelvin-Helmholtz mode. A sponge zone of 2 diameters is added to the physical domain in the outflow, where zero normal stress is enforced. The forcing space is defined on the $p$-grid. Resolvent analysis is computed using Krylov methods and LU decomposition implemented in the python package `scipy`.

For consistency, all PSD and CSD (from LES, resolvent and SLM) are expressed at reduced-order using a $N_{\text{modes}} = 50$ truncation as in (8). For LES, SPOD modes and eigenvalues are considered in the truncated series since they are the eigenfunctions and eigenvalues of the empirical CSD. In the following, only the axisymmetric mode $m = 0$ is considered, since it is the most acoustically efficient, at least for low angles. We focus in a first step on statistics of the turbulent field, and in a second step on its impact on the acoustic field.

### A. Turbulent field

Figure 2 shows the eigenvalues of the CSD matrix at $St = (0.3, 0.6, 0.9)$ from LES data (SPOD spectrum), resolvent analysis and SLM ($s_i^2$). The spectra are normalised by the first eigenvalue to free from the scaling constants inherent of linearised models. It can be noticed that resolvent analyses predict a very strong dominance of the first mode compared to the LES data. This is the sign of the obtention of strongly coherent solutions dominated by a single mode. Even if the decay rate of eigenvalues does not correspond to the SPOD spectrum, we can remark that SLM suboptimals amplitudes are larger than in resolvent analysis; and the second eigenvalue amplitude is well reproduced for a wide range of $St$.

In figure 3, the PSD (figure 3(a)) and coherence (figures 3(b), 3(c) and 3(d)) are displayed at $St = 0.7$. Concerning the PSD, we show the turbulent kinetic energy (TKE) integrated over the radial direction $TKE(x) = \int_0^R (u^2 + v^2 + w^2)\, r\, \mathrm{d}r$. It can be shown that SLM has a fair correspondence with LES compared to resolvent analyses, and we can especially remark its ability to produce a regain of kinetic energy in the downstream region, around $x = 10$, where PSD from resolvent analyses tend to decay. The figures 3(b), 3(c) and 3(d) show the coherence along the lipline $r = 0.5$ between radial velocities $v$ at $x$ and $x_c$, with $x_c = (2, 5, 8)$ respectively. Resolvent analysis, with and without eddy viscosity, predict very coherent solutions ($\gamma^2$ close to 1 for $x < 10$), while SLM leads to a very good agreement for coherence predictions.

This agreement is robust with respect to a wide range of Strouhal numbers, as shown in figure 4. We can note that classical resolvent analysis is able to produce a relevant coherence decay only for low Strouhal numbers ($St < 0.3$), when the dominance of the Kelvin-Helmholtz mode is less pronounced in resolvent analysis.

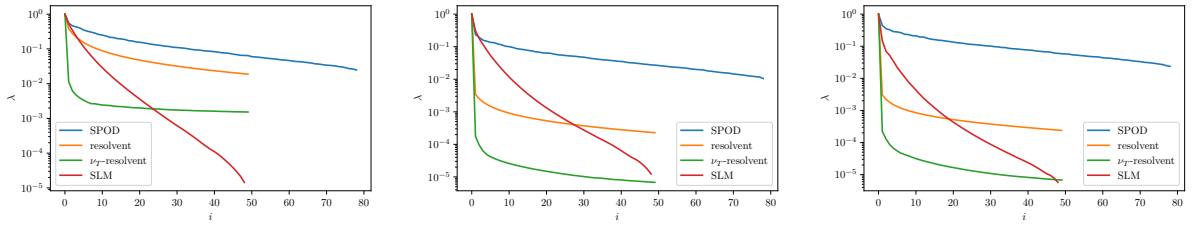


(a) $St = 0.3$ (b) $St = 0.6$ (c) $St = 0.9$

**Fig. 2 Eigenvalue spectrum of SPOD, resolvent, $\nu_T$-resolvent, and SLM. For resolvent analysis, $s_i^2$ is drawn. The spectra are normalised by the first eigenvalue.**

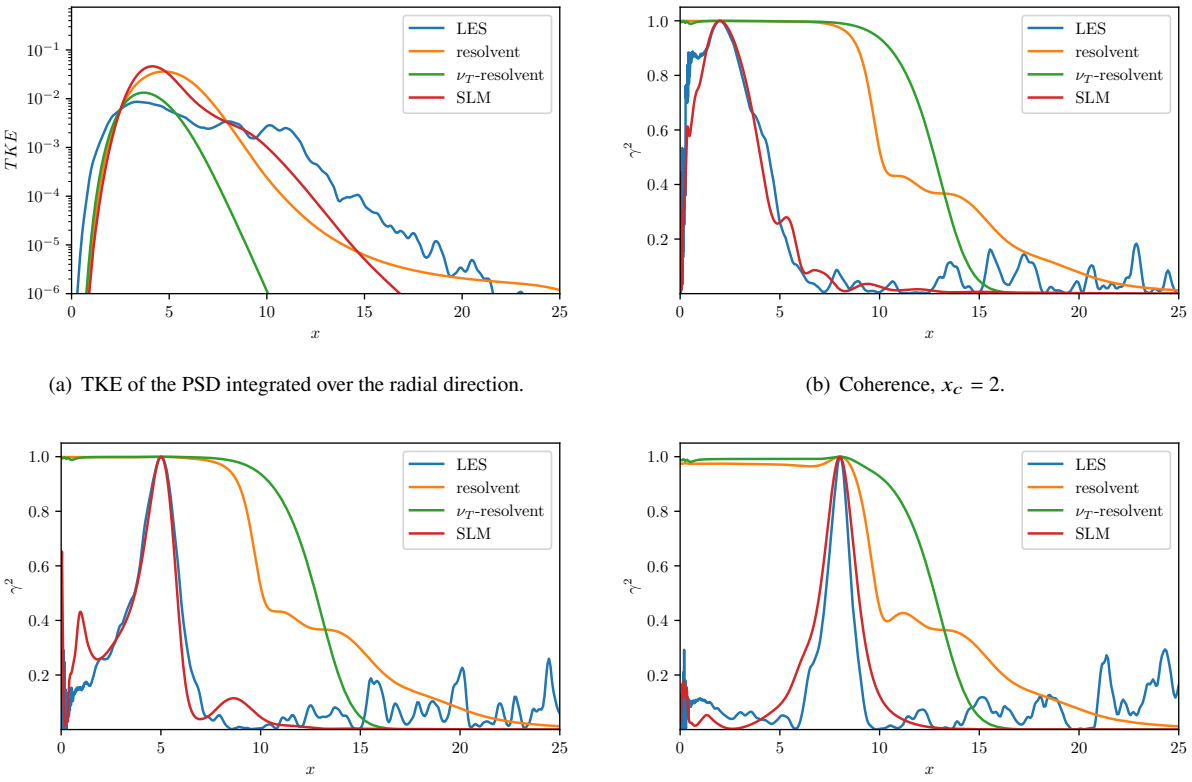


(a) TKE of the PSD integrated over the radial direction.

(b) Coherence, $x_c = 2$.

(c) Coherence, $x_c = 5$.

(d) Coherence, $x_c = 8$.

**Fig. 3 PSD and coherence $(\gamma^{vv}(x, x_c, r_c, r_c))^2$ at $St = 0.7$, with $r_c = 0.5$.**

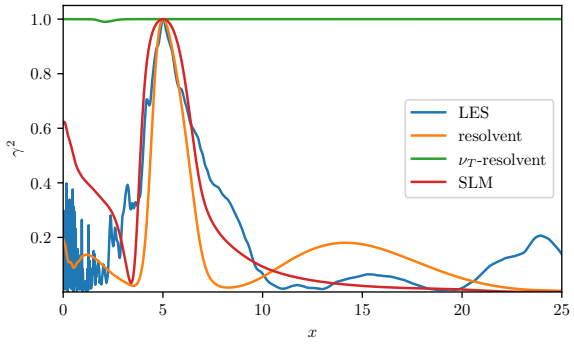


(a) $St = 0.1$.

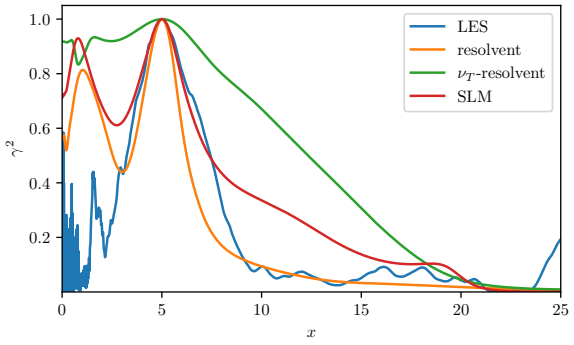


(b) $St = 0.2$.

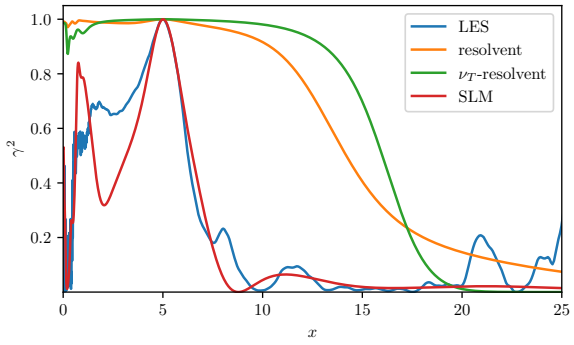


(c) $St = 0.4$.

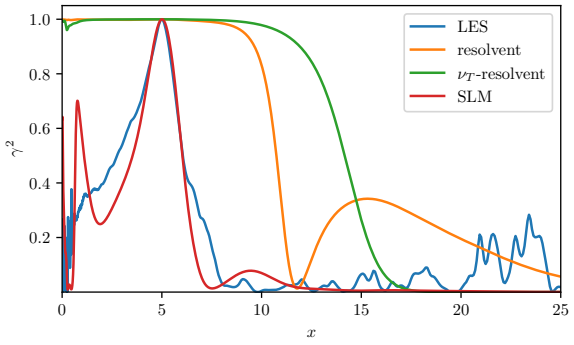


(d) $St = 0.6$.

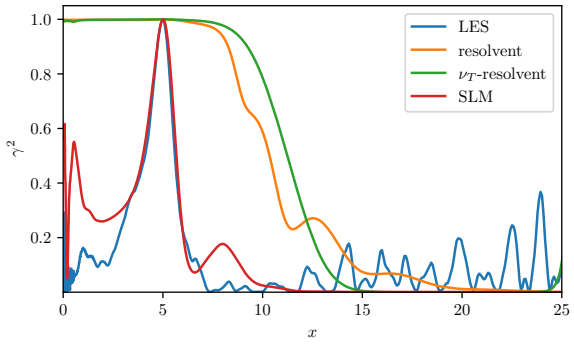


(e) $St = 0.8$.

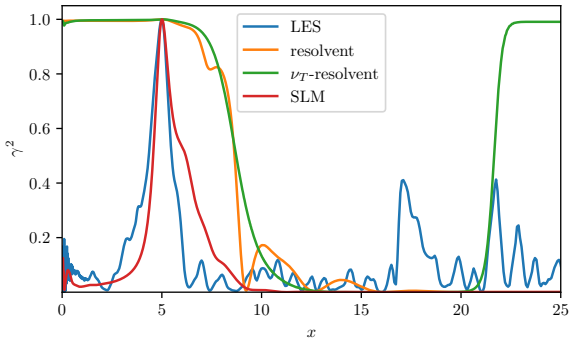


(f) $St = 1.0$.

**Fig. 4 Coherence $(\gamma^{vv}(x, x_c, r_c, r_c))^2$, with $(x_c, r_c) = (5, 0.5)$.**

As a final visualisation, resolvent/SLM modes are compared qualitatively with SPOD modes. They are eigenfunctions of the CSD and give then a picture of the variability of the predicted solution. In figure (5) the dominant mode 0 is typical of the Kelvin-Helmholtz wavepacket. The main traits of SPOD are well reproduced by all models, with a better prediction of SLM. Suboptimal modes 1 (figure 6) and mode 4 (figure 7) are also much better reproduced by SLM than resolvent analysis. Classical resolvent analysis – used to define the stochastic noise – shows clean downstream Orr-type structures, while $\nu_T$ resolvent represents well the upstream region. Combined with the fact that relative amplitudes of suboptimals are higher with SLM than resolvent, this explains the good predictions of the CSD then the coherence. Indeed, a faithful representation of the suboptimals is mandatory to make the coherence to decay in a relevant manner.

**B. Acoustic propagation**

An incompressible approximation is performed for the $M = 0.4$ jet. We propose in this section to follow the strategy of Reba et al. [25], and Baqui et al. [9], which consists in gathering the CSD of the pressure of the incompressible solution, and to propagate it by considering it as a boundary condition of a Helmholtz equation governing the acoustic field. For this, a surface has to be defined in the near-field, close enough to the jet to obtain a relevant signal, but far enough from it for the Helmholtz equation to be approximately valid. At these low Mach regimes, the results are sensitive to the domain size, choice of the surface and signal processing treatments. The objective here is to show, qualitatively and with caution, the impact of the coherence prediction on the acoustic field, and to open new perspectives of modelling.

For simplicity, we consider a cylindrical Kirchhoff surface of radius $R = 1.3D$, and the goal is to perform an acoustic propagation to $R_{ac} = 10D$. We collect the coherence envelop $\gamma$ of pressure along the surface, and consider the CSD associated with a statistical source, build on the amplitude of the dominant mode $\boldsymbol{S}^{stat}(x, x', R) = \Phi_1^p(x)\lambda_1(\Phi_1^p(x'))^*$. Conserving only the dominant mode allows to isolate the wavepacket shape, and avoid propagating small scale turbulence associated with suboptimals. A coherence-matched CSD can then be defined $\boldsymbol{S}^{match}(x, x', R) = \gamma(x, x', R)\boldsymbol{S}^{stat}(x, x', R)$. It represents a synthetic wavepacket, having the envelope of the dominant Kelvin-Helmholtz mode, but with a coherence decay representative of the solution of the stochastic model. The space Fourier-transform of the CSD $\hat{\boldsymbol{S}}^{match}(k, k', r)$ can be obtained at a radius $r = R_{ac}$, following Baqui et al. [9], by computing

$$\hat{\boldsymbol{S}}^{match}(k, k', R_{ac}) = \hat{\boldsymbol{S}}^{match}(k, k', R)h(k, R_{ac}, R, \omega)h^*(k', R_{ac}, R, \omega), \tag{19}$$

with

$$\begin{aligned} h(k, r, R, \omega) &= H_0^{(1)}\left(r\sqrt{\frac{\omega^2}{a_j^2} - k^2}\right) / H_0^{(1)}\left(R\sqrt{\frac{\omega^2}{a_j^2} - k^2}\right) \quad \text{if} \quad \omega > 0 \\ h(k, r, R, \omega) &= H_0^{(2)}\left(r\sqrt{\frac{\omega^2}{a_j^2} - k^2}\right) / H_0^{(2)}\left(R\sqrt{\frac{\omega^2}{a_j^2} - k^2}\right) \quad \text{if} \quad \omega < 0, \end{aligned} \tag{20}$$

and $H_0^{(1)}(\cdot)$, $H_0^{(2)}(\cdot)$, being the zeroth-order Hankel functions of first and second kind, respectively. In this procedure, evanescent modes are discarded. The PSD is obtained by inverse-Fourier transform of eq. (19), and gathering the diagonal of the propagated CSD. Before being Fourier-transformed, the pressure signal is windowed using a hyperbolic tangent top-hat shape, enforcing a smooth decay of the signal to zero at the boundary, with an influence on approximately 3 jet diameters from the boundary.

At $M = 0.4$ and low Strouhal numbers, only small wavenumbers are propagative. In the present study, the limited domain size reduces the range of relevant propagative modes. For this reason, we show only results at $St = 0.7$, which constitutes a good compromise between wavepacket amplification, and possibility of acoustic propagation in limited domain size. Figure (8) compares the CSD of the pressure along the cylindrical surface $R = 1.3$, between LES data, and the linear models. It highlights the ability of SLM to produce better CSD than classical and eddy resolvent analysis. In particular, we can notice the similar size of the pattern located in the upstream region ($x < 7$) associated with the wavepacket, and the presence of a narrow shape in the downstream region representing decorrelated turbulence. The maps of coherence corroborate the fact that SLM is able to predict a relevant coherence lengths, while resolvent analyses predict perfectly coherent solutions in the downstream region. To complement the study, logarithm of the absolute value of the space-Fourier transform of the CSD is displayed, superimposed with the region of propagating wavenumbers. It shows clearly that the peak associated with the wavepacket is in an evanescent region, and that an accurate modelling of

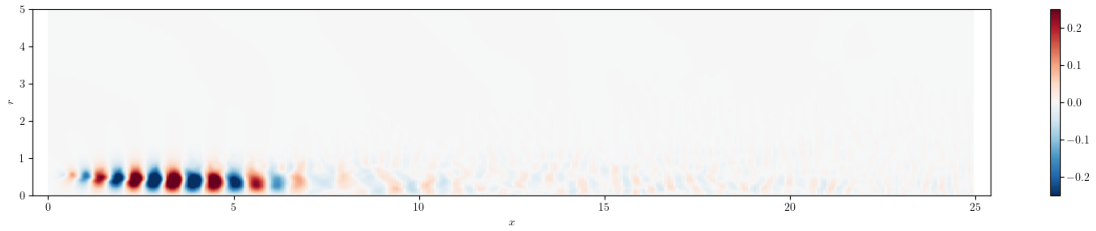


(a) SPOD.

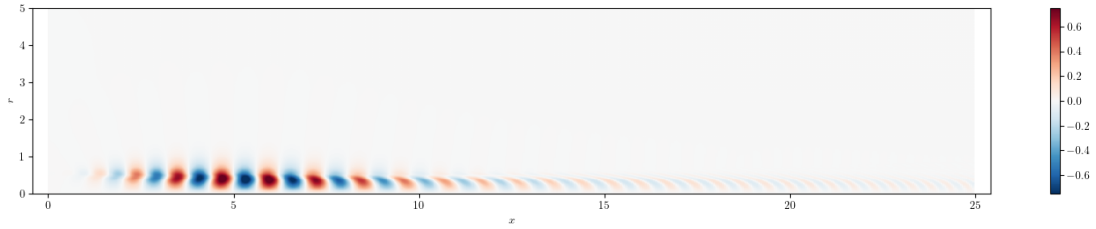


(b) Resolvent.

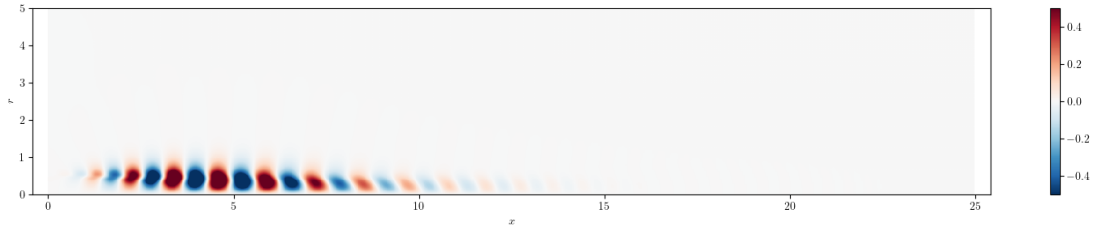


(c) $\nu_T$-resolvent.

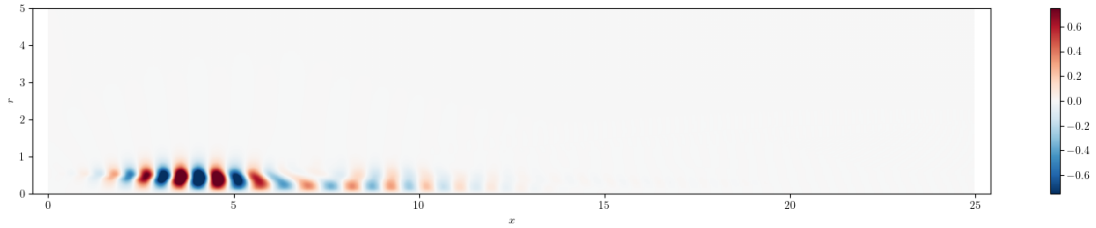


(d) SLM.

**Fig. 5 Radial velocity $v$ of mode 0 at $St = 0.7$.**

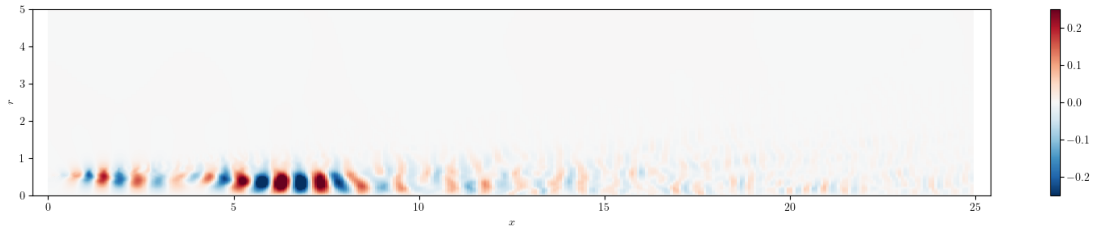


(a) SPOD.

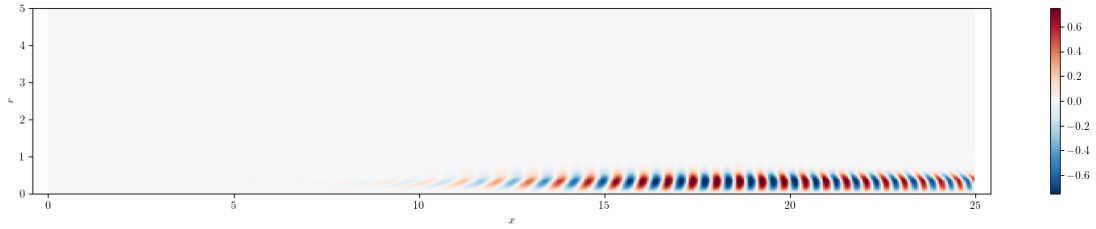


(b) Resolvent.

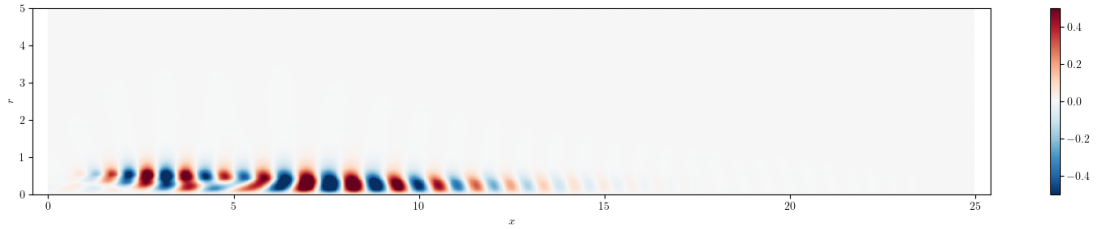


(c) $\nu_T$-resolvent.

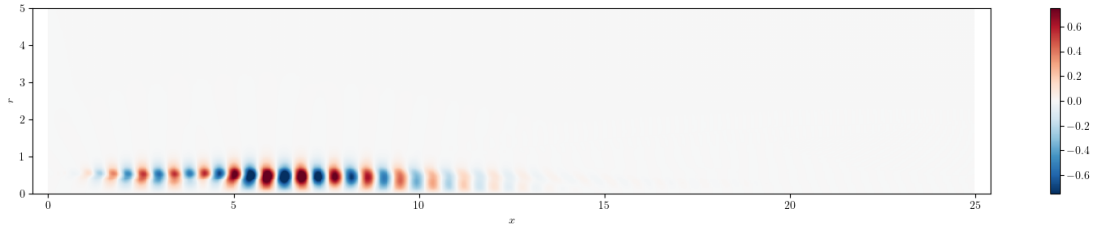


(d) SLM.

**Fig. 6 Radial velocity $v$ of mode 1 at $St = 0.7$.**

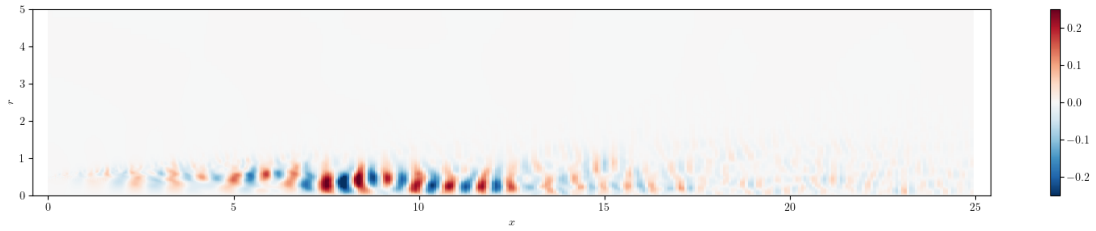


(a) SPOD.

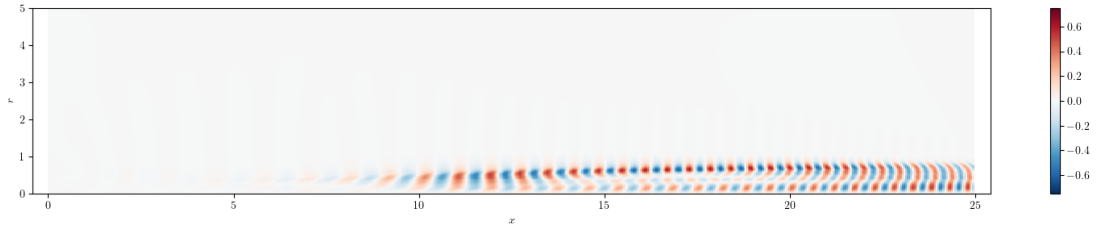


(b) Resolvent.

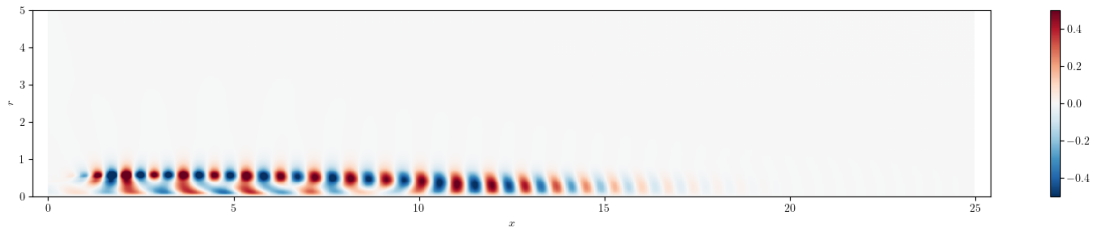


(c) $\nu_T$-resolvent.

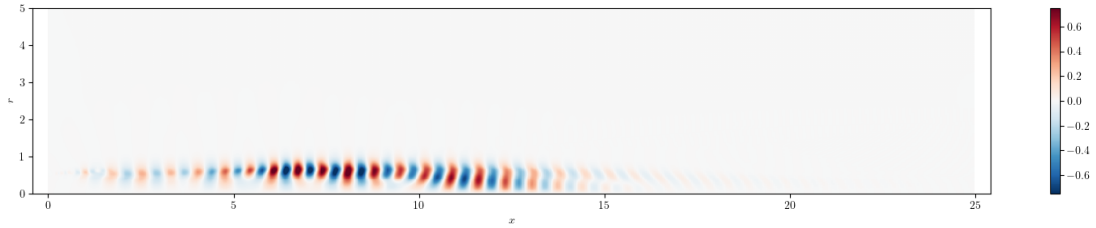


(d) SLM.

**Fig. 7 Radial velocity $v$ of mode 4, $St = 0.7$.**

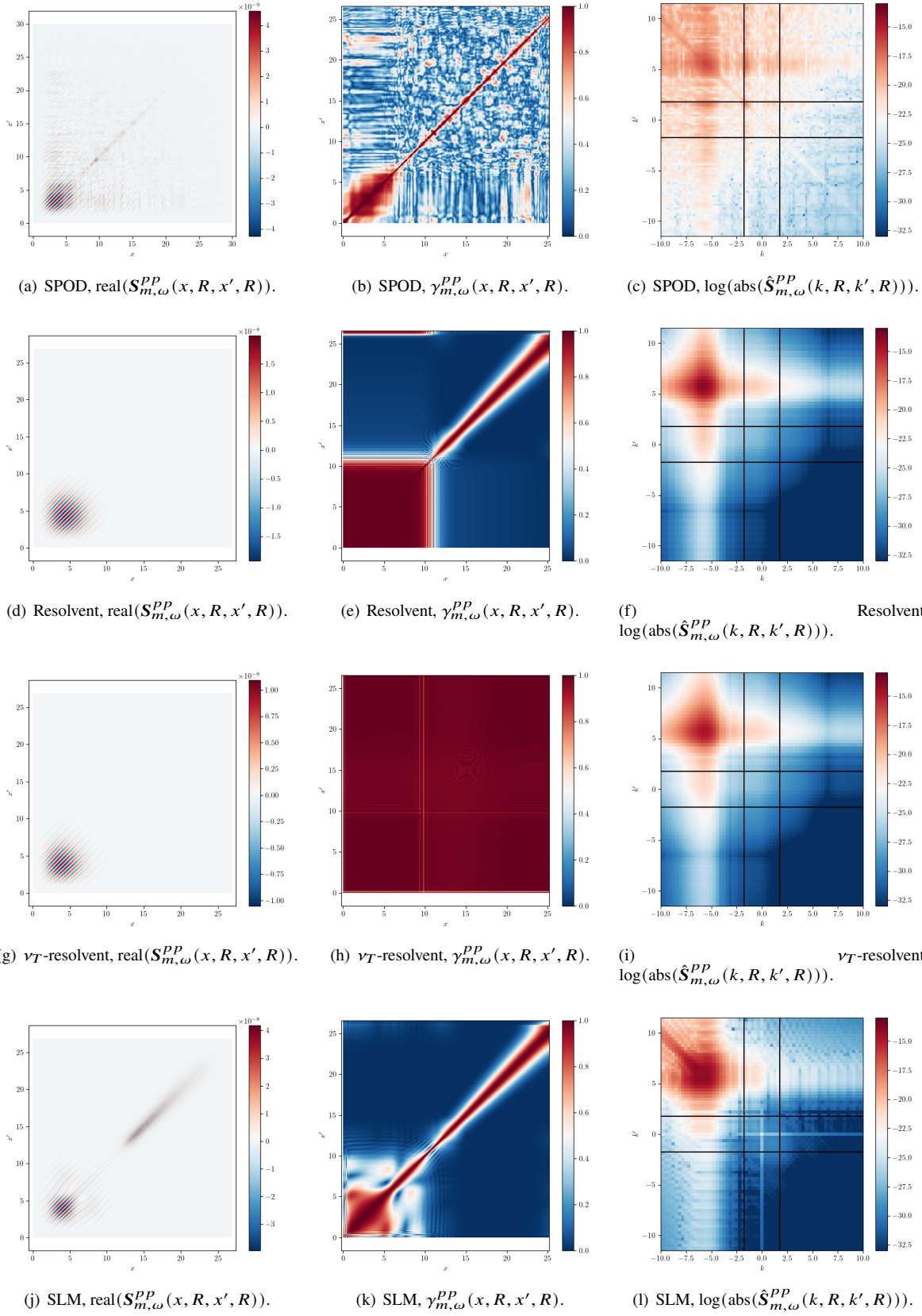

(a) SPOD, real($\boldsymbol{S}^{pp}_{m,\omega}(x, R, x', R)$). (b) SPOD, $\gamma^{pp}_{m,\omega}(x, R, x', R)$. (c) SPOD, log(abs($\hat{\boldsymbol{S}}^{pp}_{m,\omega}(k, R, k', R)$)).

(d) Resolvent, real($\boldsymbol{S}^{pp}_{m,\omega}(x, R, x', R)$). (e) Resolvent, $\gamma^{pp}_{m,\omega}(x, R, x', R)$. (f) Resolvent, log(abs($\hat{\boldsymbol{S}}^{pp}_{m,\omega}(k, R, k', R)$)).

(g) $\nu_T$-resolvent, real($\boldsymbol{S}^{pp}_{m,\omega}(x, R, x', R)$). (h) $\nu_T$-resolvent, $\gamma^{pp}_{m,\omega}(x, R, x', R)$. (i) $\nu_T$-resolvent, log(abs($\hat{\boldsymbol{S}}^{pp}_{m,\omega}(k, R, k', R)$)).

(j) SLM, real($\boldsymbol{S}^{pp}_{m,\omega}(x, R, x', R)$). (k) SLM, $\gamma^{pp}_{m,\omega}(x, R, x', R)$. (l) SLM, log(abs($\hat{\boldsymbol{S}}^{pp}_{m,\omega}(k, R, k', R)$)).

**Fig. 8 Comparisons of the pressure CSD between the LES and linear models, at $r = 1.3D$ and $St = 0.7$. Left panels: real part of the CSD, middle panels: coherence envelop, right panels: logarithm of the absolute value of the space Fourier transform of the CSD. Vertical and horizontal lines in the right panels represent the limit wavenumbers above which the wave is evanescent.**

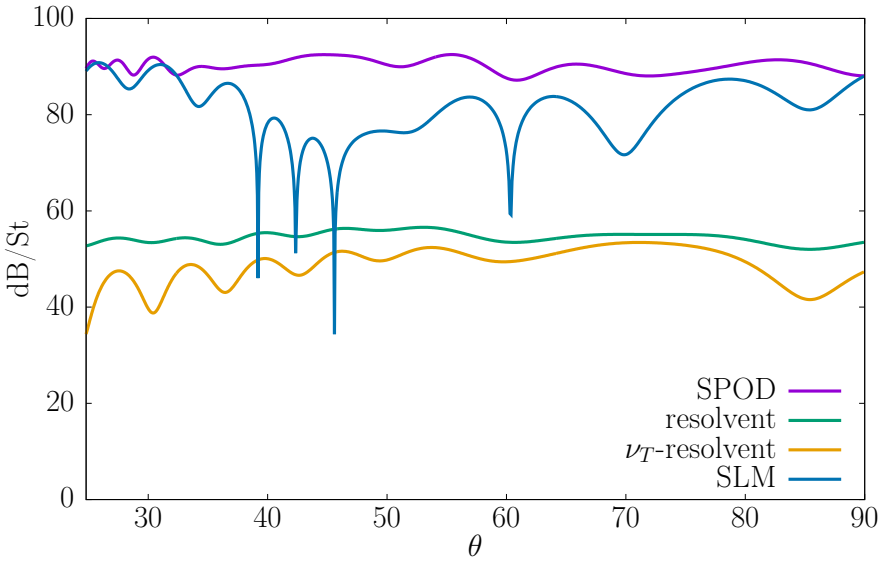


**Fig. 9 Directivity of the propagated solution from a coherence-matched statistical source, defined from LES and linear models, at $St = 0.7$.**

the tail of the spot is crucial for noise prediction. It can be seen that the shape of the CSD in the spectral space is better reproduced by SLM than resolvent.

Finally, the PSD of the propagated coherence-matched statistical wavepacket at $r = 10$ is shown in figure (9), as a function of the propagation angle, defined from the origin ($x = 0, r = 0$). The propagated solution from SPOD, resolvent, $\nu_T$-resolvent and SLM are compared. As a first caveat, we observe a directivity shape flatten compared to expected shapes. This effect has been reported in Baqui et al. [9], and is probably a consequence of the cylindrical Kirchhoff surface, which is difficult to ensure at the same time to be close enough to the jet, and assumed to be in a potential flow region. Anyway, a gap of 30 dB/$St$ between resolvent and SPOD is observed. This behaviour is consistent with the mismatch between linear models and acoustic field reported in the literature. However, SLM is able to intensify the acoustic intensity, close to the one corresponding to the propagated wavepacket extracted from LES data. This is mainly due to the ability of SLM to produce relevant coherence decay. This preliminary result, even if valid for a limited range of parameters under strong hypotheses, is demonstrative of the potential ability of stochastic modelling under location uncertainty to predict coherence decay, relevant for acoustic emissions of subsonic jets. As a consequence, it is highly encouraging to pursue in this direction, for instance by extending the modelling approach to compressible flows, in such a way to obtain acoustic emission directly from the solution of the stochastic linearised model.

## VI. Conclusion

In this paper, the stochastic modelling under location uncertainty has been employed to develop a linear stochastic model able to predict the PSD and the coherence decay of the azimuthal wavepackets in a subsonic turbulent jet. This formalism considers the conservation of mass and momentum under a stochastic transport; leading through Ito stochastic calculus to a stochastic formulation of the Navier–Stokes equations. Here, the stochastic transport aims at modelling the impact of incoherent turbulence affecting the two-point statistics of the wavepacket, and resulting of its jitter. The proposed model relies on the linearisation of the stochastic Navier–Stokes equations about the mean flow, which has been obtained by a RANS calculation. The Fourier transform of the stochastic noise is modelled by Orr-type modes produced by resolvent suboptimal modes, and the stochastic diffusion is modelled by the RANS eddy viscosity. These modelling choices allowed to produce a prediction of the CSD, leading to an enhancement of the suboptimals amplitudes and accurate comparisons with LES data of the PSD, the coherence decay and suboptimal modes (eigenfunctions of the CSD). This accordance is robust in a wide range of Strouhal numbers from $St = 0.1$ to $St = 1.0$. A Kirchhoff surface-based acoustic propagation has been preformed, demonstrating the ability of the stochastic solution to enhance the acoustic emissions.

This propagation procedure is valid in a very limited range regarding the low Mach number and the small domain

size. However, it constitutes an encouraging demonstrator, to develop stochastic modelling under location uncertainty for jet aeroacoutics. In particular, a promising perspective is to develop similar models extending the approach for compressible flows. This can be possible thanks to recent theoretical developments on stochastic modelling for compressible flows [36].

## References


[1] Jordan, P., and Colonius, T., "Wave packets and turbulent jet noise," *Annual Review of Fluid Mechanics*, Vol. 45, 2013, pp. 173–195. https://doi.org/10.1146/annurev-fluid-011212-140756.

[2] Cavalieri, A. V. G., Rodriguez, D., Jordan, P., Colonius, T., and Gervais, Y., "Wavepackets in the velocity field of turbulent jets," *Journal of Fluid Mechanics*, Vol. 730, 2013, pp. 559–592. https://doi.org/10.1017/jfm.2013.346.

[3] Rodríguez, D., Sinha, A., Brès, G. A., and Colonius, T., "Inlet conditions for wave packet models in turbulent jets based on eigenmode decomposition of large eddy simulation data," *Physics of Fluids (1994-present)*, Vol. 25, No. 10, 2013, p. 105107. https://doi.org/10.1063/1.4824479.

[4] Schmidt, O. T., Towne, A., Rigas, G., Colonius, T., and Brès, G. A., "Spectral analysis of jet turbulence," *Journal of Fluid Mechanics*, Vol. 855, 2018, p. 953–982. https://doi.org/10.1017/jfm.2018.675.

[5] Lesshafft, L., Semeraro, O., Jaunet, V., Cavalieri, A. V. G., and Jordan, P., "Resolvent-based modeling of coherent wave packets in a turbulent jet," *Physical Review Fluids*, Vol. 4, 2019, p. 063901. https://doi.org/10.1103/PhysRevFluids.4.063901.

[6] Sinha, A., Rodríguez, D., Brès, G. A., and Colonius, T., "Wavepacket models for supersonic jet noise," *Journal of Fluid Mechanics*, Vol. 742, 2014, pp. 71–95. https://doi.org/10.1017/jfm.2013.660.

[7] Cavalieri, A. V. G., Jordan, P., Agarwal, A., and Gervais, Y., "Jittering wave-packet models for subsonic jet noise," *Journal of Sound and Vibration*, Vol. 330, No. 18, 2011, pp. 4474–4492. https://doi.org/10.1016/j.jsv.2011.04.007.

[8] Cavalieri, A. V. G., and Agarwal, A., "Coherence decay and its impact on sound radiation by wavepackets," *Journal of Fluid Mechanics*, Vol. 748, 2014, pp. 399–415. https://doi.org/10.1017/jfm.2014.186.

[9] Baqui, Y. B., Agarwal, A., Cavalieri, A. V., and Sinayoko, S., "A coherence-matched linear source mechanism for subsonic jet noise," *Journal of Fluid Mechanics*, Vol. 776, 2015, p. 235–267. https://doi.org/10.1017/jfm.2015.322.

[10] Mémin, E., "Fluid flow dynamics under location uncertainty," *Geophysical & Astrophysical Fluid Dynamics*, Vol. 108, No. 2, 2014, pp. 119–146. https://doi.org/10.1080/03091929.2013.836190.

[11] Chandramouli, P., Heitz, D., Laizet, S., and Mémin, E., "Coarse large-eddy simulations in a transitional wake flow with flow models under location uncertainty," *Computers & Fluids*, Vol. 168, 2018, pp. 170–189. https://doi.org/10.1016/j.compfluid.2018.04.001.

[12] Pinier, B., Mémin, E., Laizet, S., and Lewandowski, R., "A stochastic flow approach to model the mean velocity profile of wall-bounded flows," *Physical Review E* , 2019. https://doi.org/10.1103/PhysRevE.99.063101.

[13] Yang, Y., and Mémin, E., "High-resolution data assimilation through stochastic subgrid tensor and parameter estimation from 4DEnVar," *Tellus A*, 2017, p. 19. https://doi.org/10.1080/16000870.2017.1308772.

[14] Yang, Y., and Mémin, E., "Estimation of physical parameters under location uncertainty using an Ensemble$^2$-Expectation-Maximization algorithm," *Quaterly journal of the royal meteorological society*, 2018, pp. 1–47. https://doi.org/10.1002/qj.3438.

[15] Chandramouli, P., Mémin, E., and Heitz, D., "4D large scale variational data assimilation of a turbulent flow with a dynamics error model," *Journal of Computational Physics*, Vol. 412, 2020. https://doi.org/10.1016/j.jcp.2020.109446.

[16] Resseguier, V., Mémin, E., and Chapron, B., "Geophysical flows under location uncertainty, Part I Random transport and general models," *Geophysical and Astrophysical Fluid Dynamics*, Vol. 111, No. 3, 2017, pp. 149–176. https://doi.org/10.1080/03091929.2017.1310210.

[17] Resseguier, V., Mémin, E., and Chapron, B., "Geophysical flows under location uncertainty, Part II Quasi-geostrophy and efficient ensemble spreading," *Geophysical and Astrophysical Fluid Dynamics*, Vol. 111, No. 3, 2017, pp. 177–208. https://doi.org/10.1080/03091929.2017.1312101.

[18] Resseguier, V., Mémin, E., and Chapron, B., "Geophysical flows under location uncertainty, Part III SQG and frontal dynamics under strong turbulence conditions," *Geophysical and Astrophysical Fluid Dynamics*, Vol. 111, No. 3, 2017, pp. 209–227. https://doi.org/10.1080/03091929.2017.1312102.

[19] Chapron, B., Dérian, P., Mémin, E., and Resseguier, V., "Large scale flows under location uncertainty: a consistent stochastic framework," *Quarterly Journal of the Royal Meteorological Society*, Vol. 144, No. 710, 2018, pp. 251–260. https://doi.org/10.1002/qj.3198.

[20] Bauer, W., Chandramouli, P., Chapron, B., Li, L., and Mémin, E., "Deciphering the role of small-scale inhomogeneity on geophysical flow structuration: a stochastic approach," *Journal of Physical Oceanography*, 2020. https://doi.org/10.1175/JPO-D-19-0164.1.

[21] Bauer, W., Chandramouli, P., Li, L., and Mémin, E., "Stochastic representation of mesoscale eddy effects in coarse-resolution barotropic models," *Ocean Modelling*, Vol. 151, 2020, pp. 1–50. https://doi.org/10.1016/j.ocemod.2020.101646.

[22] Tissot, G., Cavalieri, A. V. G., and Mémin, E., "Stochastic linear modes in a turbulent channel flow," *Journal of Fluid Mechanics*, Vol. 912, 2021, p. A51. https://doi.org/10.1017/jfm.2020.1168.

[23] Tissot, G., Cavalieri, A. V. G., and Mémin, E., "Input–output analysis of the stochastic Navier-Stokes equations: Application to turbulent channel flow," *Phys. Rev. Fluids*, Vol. 8, 2023, p. 033904. https://doi.org/10.1103/PhysRevFluids.8.033904.

[24] Gupta, V., Madhusudanan, A., Wan, M., Illingworth, S. J., and Juniper, M. P., "Linear-model-based estimation in wall turbulence: improved stochastic forcing and eddy viscosity terms," *Journal of Fluid Mechanics*, Vol. 925, 2021, p. A18. https://doi.org/10.1017/jfm.2021.671.

[25] Reba, R., Narayanan, S., and Colonius, T., "Wave-Packet Models for Large-Scale Mixing Noise," *International Journal of Aeroacoustics*, Vol. 9, No. 4-5, 2010, pp. 533–557. https://doi.org/10.1260/1475-472X.9.4-5.533, URL https://doi.org/10.1260/1475-472X.9.4-5.533.

[26] McKeon, B. J., and Sharma, A. S., "A critical-layer framework for turbulent pipe flow," *Journal of Fluid Mechanics*, Vol. 658, 2010, pp. 336–382. https://doi.org/10.1017/S002211201000176X.

[27] Hwang, Y., and Cossu, C., "Linear non-normal energy amplification of harmonic and stochastic forcing in the turbulent channel flow," *Journal of Fluid Mechanics*, Vol. 664, 2010, p. 51–73. https://doi.org/10.1017/S0022112010003629.

[28] Towne, A., Schmidt, O. T., and Colonius, T., "Spectral proper orthogonal decomposition and its relationship to dynamic mode decomposition and resolvent analysis," *Journal of Fluid Mechanics*, Vol. 847, 2018, pp. 821–867. https://doi.org/10.1017/jfm.2018.283.

[29] Beneddine, S., Sipp, D., Arnault, A., Dandois, J., and Lesshafft, L., "Conditions for validity of mean flow stability analysis," *Journal of Fluid Mechanics*, Vol. 798, 2016, pp. 485–504. https://doi.org/10.1017/jfm.2016.331.

[30] Reynolds, W. C., and Hussain, A. K. M. F., "The mechanics of an organized wave in turbulent shear flow. Part 3. Theoretical models and comparisons with experiments," *Journal of Fluid Mechanics*, Vol. 54, No. 2, 1972, p. 263–288. https://doi.org/10.1017/S0022112072000679.

[31] Morra, P., Semeraro, O., Henningson, D. S., and Cossu, C., "On the relevance of Reynolds stresses in resolvent analyses of turbulent wall-bounded flows," *Journal of Fluid Mechanics*, Vol. 867, 2019, p. 969–984. https://doi.org/10.1017/jfm.2019.196.

[32] Pickering, E., Rigas, G., Schmidt, O. T., Sipp, D., and Colonius, T., "Optimal eddy viscosity for resolvent-based models of coherent structures in turbulent jets," *Journal of Fluid Mechanics*, Vol. 917, 2021, p. A29. https://doi.org/10.1017/jfm.2021.232.

[33] Symon, S., Madhusudanan, A., Illingworth, S. J., and Marusic, I., "Use of eddy viscosity in resolvent analysis of turbulent channel flow," *Phys. Rev. Fluids*, Vol. 8, 2023, p. 064601. https://doi.org/10.1103/PhysRevFluids.8.064601.

[34] Tissot, G., Zhang, M., Lajús, F. C., Cavalieri, A. V. G., and Jordan, P., "Sensitivity of wavepackets in jets to nonlinear effects: the role of the critical layer," *Journal of Fluid Mechanics*, Vol. 811, 2017, pp. 95–137. https://doi.org/10.1017/jfm.2016.735.

[35] Brès, G. A., Ham, F. E., Nichols, J. W., and Lele, S. K., "Unstructured Large-Eddy Simulations of Supersonic Jets," *AIAA Journal*, Vol. 55, No. 4, 2017, pp. 1164–1184. https://doi.org/10.2514/1.J055084.

[36] Tissot, G., Mémin, E., and Jamet, Q., "Stochastic Compressible Navier–Stokes Equations Under Location Uncertainty," *Stochastic Transport in Upper Ocean Dynamics II*, Springer Nature Switzerland, Cham, 2024, pp. 293–319.